Journal of Power Sources 195 (2010) 5044–5048

Contents lists available at ScienceDirect

Journal of Power Sources

journal homepage: www.elsevier.com/locate/jpowsour

Short communication

Improvement of electrochemical behavior of Sn_2Fe/C nanocomposite anode with Al_2O_3 addition for lithium-ion batteries

Jae-Myung Lee [a], Heechul Jung [a], Yoon Hwa [a], Hansu Kim [b], Dongmin Im [b], Seok-Gwang Doo [b], Hun-Joon Sohn [a,*]

[a] Department of Materials Science and Engineering, Research Center for Energy, Conversion and Storage, Seoul National University, Seoul 151-742, Republic of Korea
[b] Energy and Environment Laboratory, Samsung Advanced Institute of Technology, Samsung Electronics, Giheung Gu, Yongin-Si, Gyeonggi-Do, 446-712, Republic of Korea

ARTICLE INFO

Article history:
Received 9 January 2010
Received in revised form 5 February 2010
Accepted 9 February 2010
Available online 1 March 2010

Keywords:
Anode
Tin-based nanocomposite
Lithium-ion battery
Alumina
Cycle performance capacity

ABSTRACT

Sn_2Fe/Al_2O_3/C nanocomposites are synthesized using a high-energy, mechanical milling method with thermally synthesized Sn_2Fe, Al_2O_3 and carbon (Super P) powders. The effect of Al_2O_3 addition on the microstructure of the Sn_2Fe/Al_2O_3/C nanocomposites is examined. The electrochemical characteristics of the material as an anode in lithium-ion batteries are also evaluated. High-resolution transmission electron microscopy shows that the crystallite size of active Sn_2Fe in the Sn_2Fe/Al_2O_3/C nanocomposite is smaller than that of the Sn_2Fe/C nanocomposite without Al_2O_3. A decrease in the initial irreversible capacity and enhanced cycle performance of the Sn_2Fe/Al_2O_3/C nanocomposite electrode are observed.

1. Introduction

Environmental pollution and the consumption of fossil fuels have driven the world to develop next-generation energy sources. Among them, lithium-ion batteries have become of great interest as power sources for mobile electric devices and electric vehicles [1–3]. At present, however, the commercial graphite-based anode has limited capacity (372 mAh g^{-1}) [4] and anode materials with high specific energy are required [1,3,5].

Tin is an attractive anode material for Li-ion batteries on account of its large gravimetric capacity, i.e., as high as 959.5 mAh g^{-1} ($Li_{17}Sn_5$). On the otherhand, the problems of capacity fading associated with Sn aggregation and extreme volume changes during the discharge–charge reaction have not been solved [6,7]. Composites consisting of an active and inactive component, nano-sized composites, amorphous materials and dispersion of the Sn particles in a carbon matrix have been examined in an attempt to solve these problems [8–13].

Following the release of Nexelion into the market by the Sony Corporation using an amorphous Sn-based composite anode consisting mainly of Sn, Co and carbon, cobalt-free Sn-transition metal alloys have attracted attention [14–20] because Co is expensive and toxic. Of these, a Sn–Fe/C composite would be a good candidate as an anode for lithium-ion batteries [21]. The Sn-Fe/C composite contains various intermetallic phases, such as Sn_2Fe, SnFe, Sn_2Fe_3, Sn_3Fe_5 and $SnFe_3$, during synthesis of the composite. The reaction mechanism of the active materials (Sn_2Fe, SnFe, and Sn_2Fe_3) has been investigated by Dahn and co-workers [15–17]. Although the Sn_2Fe/C composite shows a large specific capacity of 804 mAh g^{-1}, it still suffers from poor cycle performance and large irreversibility during the first cycle [15].

Mechanical stability is an important factor that affects the electrochemical performance of anode materials in lithium-ion batteries. During the discharge–charge reaction, a large volume change generates extreme stress and this gives rise to cracks and crumbling, as well as the loss of electrical contact within the active materials [22]. Particulate-reinforced composites are reinforced mechanically by embedding ceramic particles, which impart high tensile strength and improved resistance to crack production and propagation [23–25]. The Mohs hardness of an Al_2O_3 particle is 9 [26], and the addition of Al_2O_3 particles is expected to reinforce the Sn_2Fe/C nanocomposite materials and reduce the crystallite size of the active materials during a high-energy mechanical milling (HEMM) process.

This study examines the effect of adding Al_2O_3 particles on the microstructure of the Sn_2Fe/Al_2O_3/C nanocomposites. In addition, the electrochemical characteristics of this material as an anode in lithium-ion batteries are also evaluated using a range of analytical techniques, and the results are compared with those for Sn_2Fe/C nanocomposites.

* Corresponding author. Tel.: +82 2 880 7226; fax: +82 2 885 9671.
E-mail address: hjsohn@snu.ac.kr (H.-J. Sohn).

0378-7753/$ – see front matter © 2010 Elsevier B.V. All rights reserved.
doi:10.1016/j.jpowsour.2010.02.068

2. Experimental

Sn_2Fe/C composite materials were synthesized by means of the following process. First, a stoichiometric amount of metallic Sn (>99%, 2 μm, Aldrich) and metallic Fe (>99.9%, 3–5 μm, High purity chemicals) powders was mixed and heat-treated at 450 °C for 12 h under an argon atmosphere at a heating rate of 0.08 °C s^{-1}, followed by cooling to room temperature. The thermally synthesized Sn_2Fe and C (Super P) powders at a ratio of 85:15 wt.% were mixed in a hardened steel vial with a ball-to-powder ratio of 20:1. A vial, which was assembled in an argon-filled glove-box, was placed on a laboratory-made vibratory mill and milled at a rotation speed of 500 rpm for 40 h.

The Sn_2Fe/Al_2O_3/C nanocomposite materials were prepared as follows. The thermally synthesized Sn_2Fe, Al_2O_3 (<50 nm, Aldrich) and C (Super P) powders with various Sn_2Fe:Al_2O_3:C ratios were mixed in a hardened steel vial with a ball-to-powder ratio of 20:1. A similar vial prepared using the above-mentioned method was placed on a laboratory-made vibratory mill and milled at a rotation speed of 500 rpm for 40 h. The final products were ground and sieved to obtain particles of <38 μm in size. Preliminary tests showed that the optimum conditions for the HEMM process for cycle performance and first cycle efficiency was a rotation speed and milling time of 500 rpm and 40 h, respectively.

The test electrodes consisted of the active powder material (70 wt.%), Super P (15 wt.%) as a conducting agent and polyvinylidene fluoride (PVDF, 15 wt.%) dissolved in N-methyl pyrrolidinone (NMP) as a binder. All these components were well-mixed using a magnetic stirrer to form a slurry. The slurry was coated on a copper foil substrate by means of doctor blade, pressed and dried at 120 °C for 4 h under a vacuum. A laboratory-made coin-type cell was used with lithium foil as the counter and reference electrodes and 1 M $LiPF_6$ in ethylene carbonate (EC)/diethylene carbonate (DEC) (1:1, vol.%, Samsung) as the electrolyte. The cell assembly and all electrochemical tests were carried out in an argon-filled glove-box. The discharge/charge experiments were performed galvanostatically within a voltage window of 0.0–1.5 V (vs. Li/Li^+) at a current of 100 mA g^{-1}.

The phase composition of the synthesized powders was examined by X-ray diffraction (XRD, Rigaku, D-MAX2500-PC). The particle size, morphology, microstructure, and crystallite size of synthesized powders were characterized by scanning electron microscopy (SEM, JEOL, JSM-6360) and by high-resolution transmission electron microscopy (HRTEM, JEOL, JEM-3000F).

3. Results and discussion

The XRD patterns and SEM images of the pure Sn_2Fe, the Sn_2Fe/C composite and the Sn_2Fe/Al_2O_3/C composite are presented in Fig. 1. All the peaks correspond to the Sn_2Fe (JCPDS #03-065-0374) phase without any other phases and the particle size of the Sn_2Fe powders is approximately 5–8 μm, as shown in Fig. 1a. Although the Sn_2Fe peaks in the Sn_2Fe/C composite and Sn_2Fe/Al_2O_3/C composite are broadened due to the HEMM process (Fig. 1b and c), all the diffraction peaks coincided with Sn_2Fe phases. No Al_2O_3 peaks are observed due to the small quantity of this material. The particle size of Sn_2Fe in Sn_2Fe/C and in Sn_2Fe/Al_2O_3/C composite is <3 μm.

Bright-field TEM and HRTEM with fast Fourier transformed (FT) images of the Sn_2Fe/C composite and the Sn_2Fe/Al_2O_3/C composite materials with different wt.% of each component are shown in Fig. 2. The Sn_2Fe phase that had previously been identified by XRD is confirmed by the FT images in Fig. 2a. The crystallite size of the Sn_2Fe/C composite materials is approximately 15–25 nm. The Sn_2Fe (solid circle) and Al_2O_3 (dotted circle) phases can be identified in the bright-field TEM and HRTEM with the fast Fourier transformed (FT) images of the Sn_2Fe/Al_2O_3/C (wt.% of Sn_2Fe:Al_2O_3:C = 84:1:15) composites in Fig. 2b. The crystallite size of Sn_2Fe in the composite is reduced to approximately 8–15 nm. In addition, the size of Al_2O_3 is approximately 6–10 nm. Fig. 2c and d shows the bright-field TEM and HRTEM with the fast Fourier transformed (FT) images of the Sn_2Fe/Al_2O_3/C composites with Sn_2Fe:Al_2O_3:C = 82:3:15 and 80:5:15 in wt.%, respectively. The HRTEM images reveal that the Sn_2Fe crystallites and Al_2O_3 are dispersed uniformly in the amorphous carbon matrix. The crystallite size of Sn_2Fe in the Sn_2Fe/Al_2O_3/C nanocomposite materials is reduced further to approximately 5–10 nm for both nanocomposites. The addition of Al_2O_3 particles therefore plays a role in the random dispersion of Sn_2Fe crystallites as well as a decrease in the crystallite size of the active materials. The size of the Sn_2Fe crystallites is similar in both nanocomposites. Therefore, the electrochemical tests were performed using the Sn_2Fe/Al_2O_3/C nanocomposite materials containing 3 wt.% of Al_2O_3 because the size of Sn_2Fe crystallites is similar for both nanocomposites.

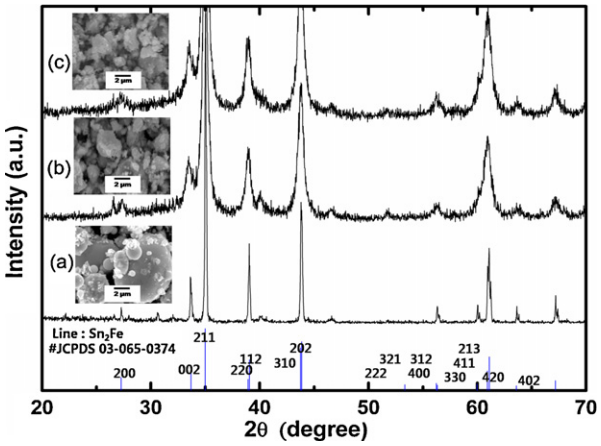

Fig. 1. XRD patterns and SEM images of (a) pure Sn_2Fe, (b) Sn_2Fe/C (wt.% of Sn_2Fe:C = 85:15) composite and (c) Sn_2Fe/Al_2O_3/C (wt.% of Sn_2Fe:Al_2O_3:C = 82:3:15) composite.

Fig. 3a shows the discharge–charge voltage profiles of the Sn_2Fe/Al_2O_3 (3 wt.%)/C nanocomposite electrode for the 1, 2, 10, 20 and 30 cycles at a constant current of 100 mA g^{-1} over a voltage range of 0.0–1.5 V (vs. Li/Li^+). The shape of the voltage profiles is similar except for the first cycle. The discharge and charge capacities of the Sn_2Fe/Al_2O_3/C nanocomposite electrode during the first cycle are 824 and 654 mAh g^{-1}, respectively, and the initial coulombic efficiency is almost 80%. The discharge and charge capacities of the first cycle for the pure milled carbon electrode are 1009 and 412 mAh g^{-1}, respectively. Since the Sn_2Fe/Al_2O_3 (3 wt.%)/C nanocomposite contains 15 wt.% carbon, it contributes 151 mAh g^{-1} to the first discharge capacity, and 90 mAh g^{-1} to the initial irreversible capacity. The coulombic efficiency for the second cycle is increased to 97%.

Differential capacity plots (DCPs) of the Sn_2Fe/Al_2O_3(3 wt.%)/C nanocomposite electrode are presented in Fig. 3b. In addition, Fig. 3c shows the ex situ XRD patterns of the Sn_2Fe/Al_2O_3 (3 wt.%)/C nanocomposite electrode for a given potential, as indicated the DCP during the first cycle along with the second cycles at 1.5 V. During the first discharge process, a solid electrolyte interphase (SEI) forms on the surfaces of the active material near 0.75 V as the electrolyte is decomposed [27]. The alloying of Sn and carbon with lithium occurs at a potential below 0.6 V to form various Li_xSn ($x < 4.4$) alloys and Li_yC. In addition, the broad peak near 0.12 V in the DCP for the first cycle is due mainly to Li insertion into the amorphous carbon present in the composite. The Bragg peaks of the Sn_2Fe phase disappear at 0.0 V and the $Li_{4.4}Sn$ peak appears. During charging,

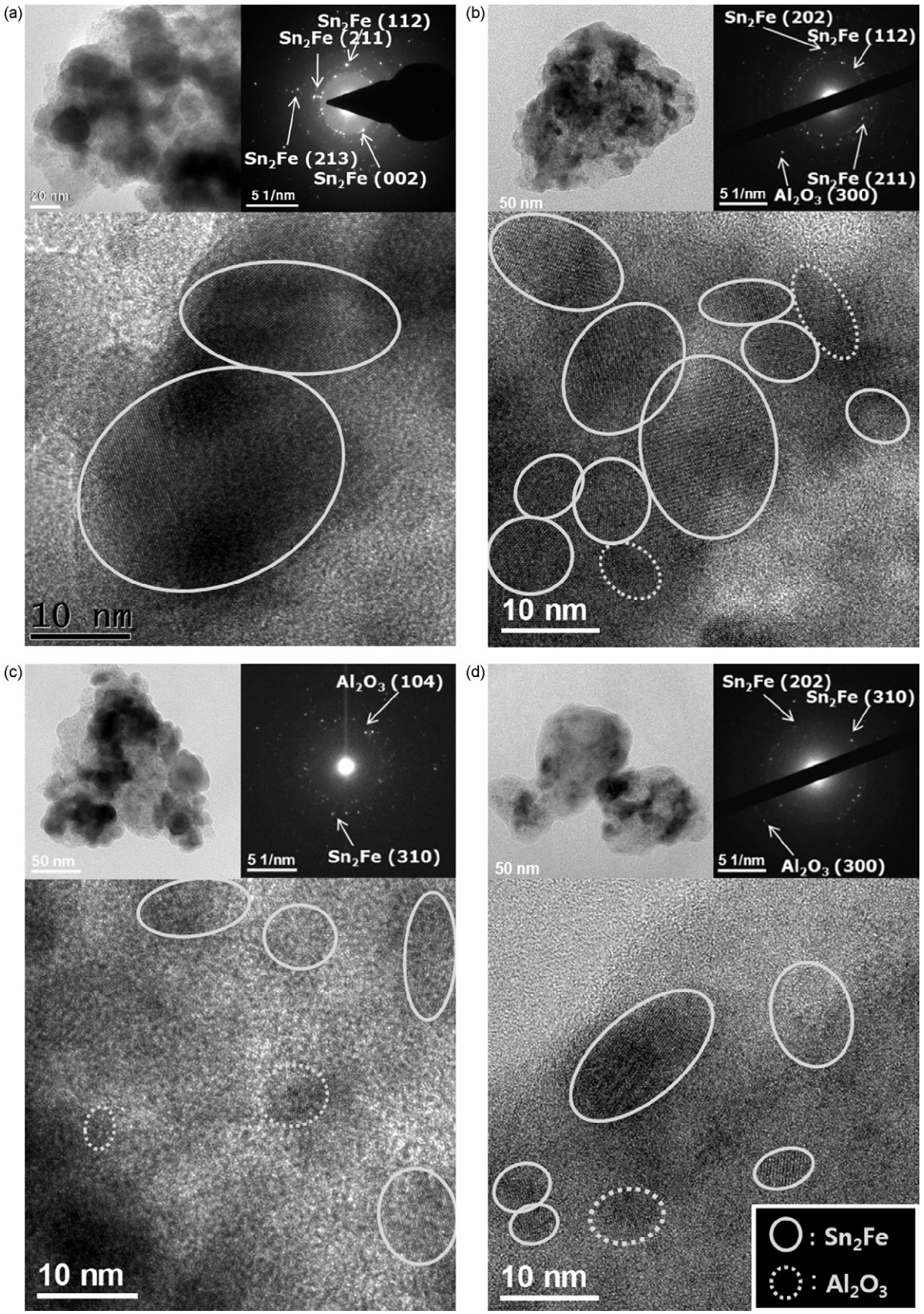

Fig. 2. HRTEM and FT images of (a) Sn_2Fe/C (wt.% of Sn_2Fe:C = 85:15) nanocomposite $Sn_2Fe/Al_2O_3/C$ (wt.% of (b) 84:1:15, (c) 82:3:15, and (d) 80:5:15) nanocomposite before cycling test (○: Sn_2Fe; ◌: Al_2O_3).

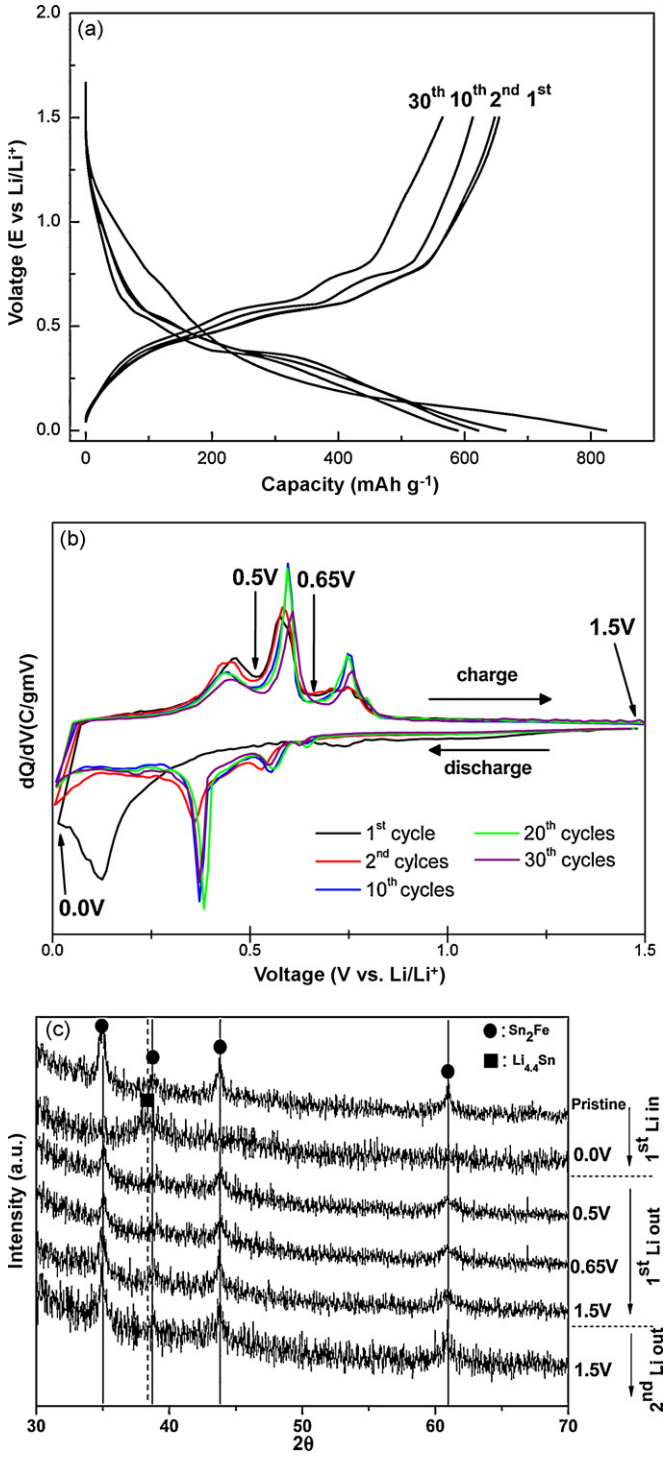

Fig. 3. (a) Discharge–charge voltage profiles for 1, 2, 10, 20 and 30 cycles and (b) DCPs, (c) ex situ XRD patterns of $Sn_2Fe/Al_2O_3/C$ (wt.% of 82:3:15) nanocomposite at selected potentials during first cycle and fully charged state (1.5 V) at second cycle.

the Li–Sn alloys decompose and Sn atoms aggregate to form large Sn clusters at approximately 0.75 V, as suggested by Courtney and Dahn [28] and identified by Retoux et al. [29] and Kim et al. [7]. In the presence of Fe released during the discharge step [15], however, Sn recombines with Fe to form the Sn_2Fe phase which prevents the aggregation of Sn atoms, as shown in the XRD pattern in Fig. 3c. This recombination reaction provides better cycleability than a pure tin electrode. After the first discharge, the DCPs became similar in subsequent cycles, and are almost the same as that of metallic Sn [28].

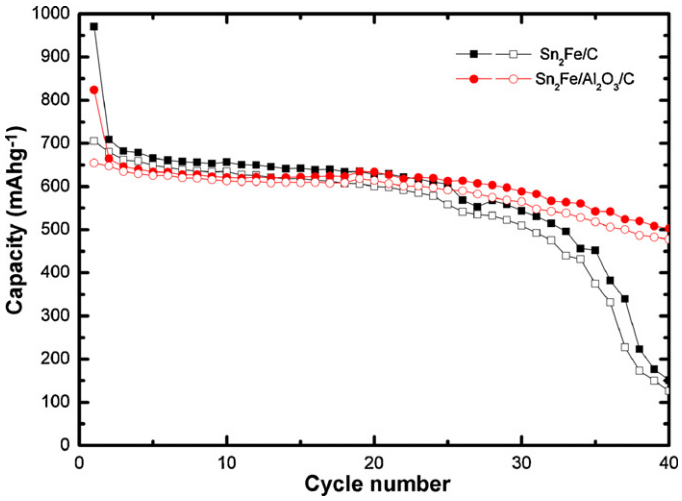

Fig. 4. Cycle performance of Sn_2Fe/C nanocomposite (wt.% of Sn_2Fe:C = 85:15) and $Sn_2Fe/Al_2O_3/C$ (wt.% of 82:3:15) nanocomposite electrodes.

After the tenth cycle, the DCPs profiles are similar and these by indicate the reversibility of the discharge–charge process. This might be related to the presence of liberated Fe atoms, which will act as an inactive matrix to suppress the aggregation of Sn atoms and amorphous carbon accommodates the volume change during cycling [21].

The cycle performance of the Sn_2Fe/C nanocomposite electrode is compared with that of the Sn_2Fe/Al_2O_3(3 wt.%)/C nanocomposite electrode in Fig. 4; the irreversible capacities during the first cycle are 265 and 170 mAh g^{-1}, respectively. Although the capacity for the Sn_2Fe/C nanocomposite electrode fades rapidly after the 20th cycle, the Sn_2Fe/Al_2O_3(3 wt.%)/C nanocomposite electrode shows enhanced cycle performance. In addition, the reversible charge capacity of the Sn_2Fe/Al_2O_3(3 wt.%)/C nanocomposite electrode is 477 mAh g^{-1} (73% of its initial charge capacity) after 40 cycles compared with 126 mAh g^{-1} (18% of the initial charge capacity) for the Sn_2Fe/C nanocomposite electrode. As mentioned above, a decrease in initial irreversible capacity and an enhanced cycle performance are found for the Sn_2Fe/Al_2O_3(3 wt.%)/C nanocomposite electrode. These improvements are attributed to a decrease in crystallite size [30–33], uniform dispersion of the active material and greater mechanical stability of the particulate-reinforced composite through the embedding of Al_2O_3 [22].

4. Conclusions

$Sn_2Fe/Al_2O_3/C$ nanocomposites have been synthesized by mechanical milling of thermally synthesized Sn_2Fe, Al_2O_3 powder and carbon. Pure Sn_2Fe is produced by a thermal reaction between metallic Sn and Fe powders. The Sn_2Fe/Al_2O_3(3 wt.%)/C nanocomposites are examined as anode materials for lithium-ion batteries. The Sn_2Fe/Al_2O_3(3 wt.%)/C nanocomposite electrode shows a decrease in initial irreversible capacity and enhanced cycle performance, which are attributed to a decrease in crystallite size and uniform dispersion of the active materials. The superior mechanical stability and consequent improved cycle performance of the particulate-reinforced composite is due to the embedded Al_2O_3.

Acknowledgements

This study was supported by Samsung Advanced Institute of Technology and the Korea Science and Engineering Foundation (KOSEF) through the Research Center for Energy Conversion and

Storage at Seoul National University (Grant No. R11-2002-102-02001-0).

References

[1] M. Winter, J.O. Besenhard, M.E. Spahr, P. Novak, Adv. Mater. 10 (1998) 725.
[2] P. Poizot, S. Laruelle, S. Grugeon, L. Dupont, J.M. Tarascon, Nature 407 (2000) 496.
[3] A.S. Aricò, P. Bruce, B. Scrosati, J.M. Tarascon, W. Van Schalkwijk, Nat. Mater. 4 (2005) 366.
[4] R.A. Huggins, J. Power Sources 81 (1993) 13.
[5] R.A. Huggins, in: G.-A. Abbas, G. Pistoia (Eds.), Lithium Batteries, Kluwer Academic Publishers, Boston, 2004, p. 270.
[6] M. Winter, J.O. Besenhard, Electrochim. Acta 45 (1999) 31.
[7] J.-H. Kim, G.-J. Jeong, Y.-W. Kim, H.-J. Sohn, C.W. Park, C.K. Lee, J. Electrochem. Soc. 150 (2003) A1544–A1547.
[8] A.D.W. Todd, R.E. Mar, J.R. Dahn, J. Electrochem. Soc. 154 (2007) 597.
[9] I.-S. Kim, P.N. Kumta, G.E. Blomgren, Electrochem. Solid State Lett. 3 (2000) 493.
[10] S. Bourderau, T. Brousse, D.M. Schleich, J. Power Sources 81 (1999) 233.
[11] S. Yoon, S.-I. Lee, H. Kim, H.-J. Sohn, J. Power Sources 161 (2006) 1319.
[12] O. Mao, R.L. Turner, I.A. Courtney, B.D. Fredericksen, M.I. Buckett, L.J. Krause, J.R. Dahn, Electrochem. Solid State Lett. 2 (1999) 3.
[13] J. Hassoun, G. Derrien, S. Panero, B. Scrosati, Adv. Mater. 20 (2008) 3169.
[14] http://www.sony.net/SonyInfo/News/Press/200502/05-006E/index.html.
[15] O. Mao, R.A. Dunlap, J.R. Dahn, J. Electrochem. Soc. 146 (1999) 405.
[16] O. Mao, J.R. Dahn, J. Electrochem. Soc. 146 (1999) 414.
[17] O. Mao, J.R. Dahn, J. Electrochem. Soc. 146 (1999) 423.
[18] A.D.W. Todd, R.E. Mar, J.R. Dahn, J. Electrochem. Soc. 153 (2006) A1998.
[19] A.D.W. Todd, R.E. Mar, J.R. Dahn, J. Electrochem. Soc. 154 (2007) A597.
[20] H. Hassoun, S. Panero, G. Mulas, B. Scrosati, J. Power Sources 171 (2007) 928.
[21] S. Yoon, J.-M. Lee, H. Kim, D. Im, S.-G. Doo, H.-J. Sohn, Electrochim. Acta 54 (2009) 2099.
[22] G.-J. Jeong, Y.U. Kim, H.-J. Sohn, T. Kang, J. Power Sources 101 (2001) 201.
[23] D.L. Davidson, in: R.K. Everett, R.J. Arsenault (Eds.), Metal Matrix Composites: Mechanisms and Properties, Academic Press, San Diego, CA, 1991, p. 217.
[24] D.L. Chen, M.C. Chaturvedi, N. Goel, N.L. Richards, Int. Fatigue 21 (1999) 1079.
[25] M.S. El-Eskandarany, J. Alloys Compd. 279 (1998) 263.
[26] http://www.rpi.edu/~schubert/Educational-resources/Materials-Hardness.pdf.
[27] W.-R. Liu, J.-H. Wang, H.-C. Wu, D.-T. Shieh, M.-H. Yang, N.-L. Wu, J. Electrochem. Soc. 152 (2005) A1719.
[28] I.A. Courtney, J.R. Dahn, J. Electrochem. Soc. 144 (1997) 2045.
[29] R. Retoux, T. Brousse, D.M. Schleich, J. Electrochem. Soc. 146 (1999) 2472.
[30] J.H. Ahn, Y.J. Kim, G.X. Wang, M. Lindsay, H.k. Liu, S.X. Dou, Mater. Trans. 43 (2002) 63.
[31] C. Suryanarayana, Prog. Mater. Sci. 46 (2001) 1.
[32] T. Ambrose, A. Gavin, C.L. Chien, J. Magn. Magn. Mater. 116 (1992) L311.
[33] J. Yang, Y. Takeda, N. Imanishi, O. Yamamoto, J. Electrochem. Soc. 146 (1999) 4009.